

Rapid long-range disynaptic inhibition explains the formation of cortical orientation maps.

Ján Antolík^{1,*}

¹ Unité de Neurosciences, Information et Complexité, CNRS UPR 3293, Gif-sur-Yvette, France

Correspondence*:

Ján Antolík
antolikjan@gmail.com

2 ABSTRACT

3

4 Competitive interactions are believed to underlie many types of cortical processing, ranging
5 from memory formation, attention and development of cortical functional organization (e.g.
6 development of orientation maps in primary visual cortex). In the latter case, the competitive
7 interactions happen along the cortical surface, with local populations of neurons reinforcing each
8 other while competing with those displaced more distally. This specific configuration of lateral
9 interactions is however in stark contrast with the known properties of the anatomical substrate,
10 i.e. excitatory connections (mediating reinforcement) having longer reach than inhibitory ones
11 (mediating competition). No satisfactory biologically plausible resolution of this conflict between
12 anatomical measures, and assumed cortical function has been proposed. Recently a specific
13 pattern of delays between different types of neurons in cat cortex has been discovered, where
14 direct mono-synaptic excitation has approximately the same delay, as the combined delays of
15 the disynaptic inhibitory interactions between excitatory neurons (i.e. the sum of delays from
16 excitatory to inhibitory and from inhibitory to excitatory neurons). Here we show that this specific
17 pattern of delays represents a biologically plausible explanation for how short-range inhibition
18 can support competitive interactions that underlie the development of orientation maps in primary
19 visual cortex. We demonstrate this statement analytically under simplifying conditions, and
20 subsequently show using network simulations that development of orientation maps is preserved
21 when long-range excitation, direct inhibitory to inhibitory interactions, and moderate inequality in
22 the delays between excitatory and inhibitory pathways is added.

23 **Keywords:** primary visual cortex, rate model, cortical functional development, Hebbian learning, cortical horizontal connectivity,
24 orientation map

25 ??

1 INTRODUCTION

Competition between populations of neurons has been proposed as one of the canonical computations of cortical networks, and has been hypothesized to underly a range of brain functions including working memory (Amit and Brunel, 1995; Durstewitz et al., 2000), orientation tuning (Somers et al., 1995; Ben-Yishai et al., 1995), and functional map development (von der Malsburg, 1973; Miikkulainen et al., 2005; Antolík and Bednar, 2011). In developmental models of functional cortical organization the competition occurs between populations of neurons spatially offset along the cortical surface, whereby local populations mutually reinforce each other via excitatory connections (short-range excitation) while long-range inhibition facilitates competition between the local populations and stabilizes the activity in the network. Such so called Mexican-hat arrangement of recurrent interactions (figure 1A), however, is in stark contrast to the known anatomical arrangement of cortical circuitry: the excitatory neurons (especially in superficial layers) tend to form long-range arborizations spanning multiple columns while the axons of a majority of inhibitory neurons are confined to an area only several hundreds of micrometers in diameter (Buzás et al., 2006; Budd and Kisvárday, 2001) (figure 1B).

As pointed out by Muir *et al.* in their recent study (Muir and Cook, 2014), to solve this apparent conflict, previous topologically organized models of cortical competition have either relied on the anatomically unsupported Mexican-hat profile of lateral interactions (von der Malsburg, 1973; Miikkulainen et al., 2005), or relied on other biologically unrealistic properties, such as selective targeting of inhibitory neurons by long range excitatory connections (Law, 2009; Rutishauser et al., 2012) or instantaneous synaptic transmission coupled with omission of recurrent inhibition (Kang et al., 2003; Levy and Reyes, 2011; Grabska-Barwinska and von der Malsburg, 2008).

A common hypothesis about how to reconcile Mexican-hat lateral interactions with anatomical reality is that the range of the effective inhibitory influence of an excitatory neuron onto other excitatory neurons (via the disynaptic pathway from excitatory to inhibitory to excitatory neurons - the disynaptic inhibition) will correspond to the cumulative reach of the direct excitatory and the direct inhibitory connections. The effective inhibitory interactions between excitatory neurons will thus have longer range than the direct excitatory connections, supporting the use of Mexican-hat lateral interactions in population models (i.e. models without explicit separation of excitatory and inhibitory populations). Even though very intuitive, this explanation has never been explicitly demonstrated, and it omits the fact that under the reasonable null hypothesis of equal transmission delays for all connections, the recurrent disynaptic inhibition will lag the direct recurrent excitation. As it turns out this is crucial, as recent model analysis by Muir *et al.* (Muir and Cook, 2014) shows that, under the assumption of uniform transmission delays, the presence of competition across the cortical surface is predicted well by the anatomy of direct excitatory and inhibitory coupling and that multi-synaptic network effects are negligible, effectively rejecting the disynaptic explanation behind Mexican-hat interaction. In conclusion, currently no satisfactory explanation of how topological functional organization develops in cortical networks that is consistent with the present anatomical findings exists.

As we will show in this study, the nature of the transmission delays between different neural type (excitatory,inhibitory) combinations holds the key to resolving this long standing open question. A recent study by Ohana *et al.* (Ohana et al., 2012) revealed a specific pattern of transmission delays between different neural type combinations. Specifically they found that the excitatory to excitatory connections are slow while the excitatory to inhibitory connections are fast. In this study we explore the possibility that this specific transmission delay pattern is the missing link that can explain how short range inhibition can lead to effective cortical competition. We employ computational models to show that the fast excitatory-to-inhibitory-to-excitatory pathway allows for the disynaptic inhibition to generate the effective Mexican-hat

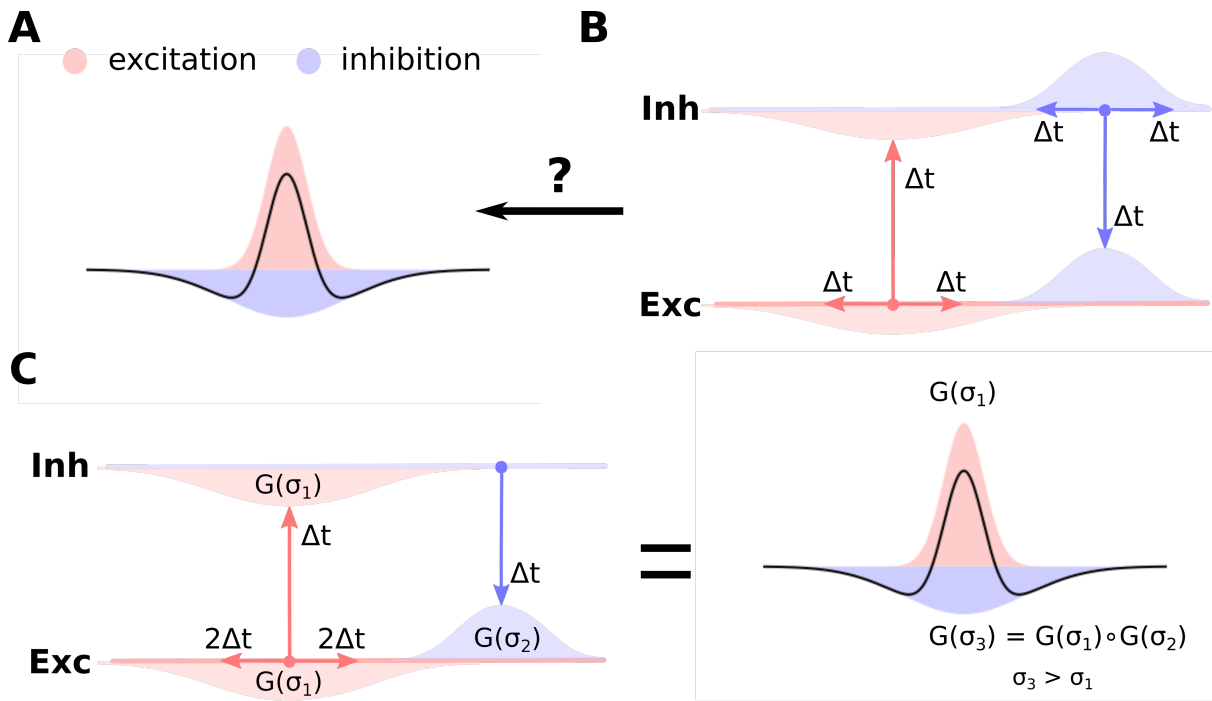


Figure 1. Cortical anatomy and effective lateral interactions. (A) Short-range excitation (red) and long-range inhibition (blue) leads to effective Mexican-hat lateral interactions (black curve). (B) Anatomical evidence indicates the oposite organization of lateral connectivity in cortex, whereby excitatory neurons send long-range connections to other neurons, while inhibitory neurons only local ones. Furthermore, uniform delays accross the intra-cortical projections is tipically assumed. It is not clear how such anatomical configuration can support the Mexican-hat effective interaction across cortical surface. (C) Under the assumption of slow excitatory-to-excitatory and fast excitatory-to-inhibitory and inhibitory-to-excitatory pathway (and disregarding the inhibitory-to-inhibitory interactions), the effective lateral inhibitory interactions correspond to the convolution of the excitatory-to-inhibitory and inhibitory-to-excitatory connection kernels. Under the assumption that these kernels are Gaussian ($G(\sigma)$ in the figure), the effective inhibitory interactions will be Gaussian with variance (space-constant) greater than the excitatory-to-excitatory one, thus forming Mexican-hat lateral interaction profile.

69 like lateral interactions (figure 1C), thus for the first time explaining competition in topologically organized
 70 cortical networks with no biologically implausible assumptions. To demonstrate the proposed properties, in
 71 this study we focus on models of development of orientation maps, because this is the most well explored
 72 example of competition driven functional cortical organization development, but these results generalize
 73 to development of other cortical topological properties, as well as potentially other competition based
 74 computations.

2 MATERIALS AND METHODS

75 Here we describe the two models and their variants used in this study and finish with a description of a
 76 measure for assessing the extent to which model orientation maps resemble their biological counterparts.
 77 Since this study heavily leans on methodology developed in our previous studies, we offer here a short
 78 description and refer readers to the original articles for the details.

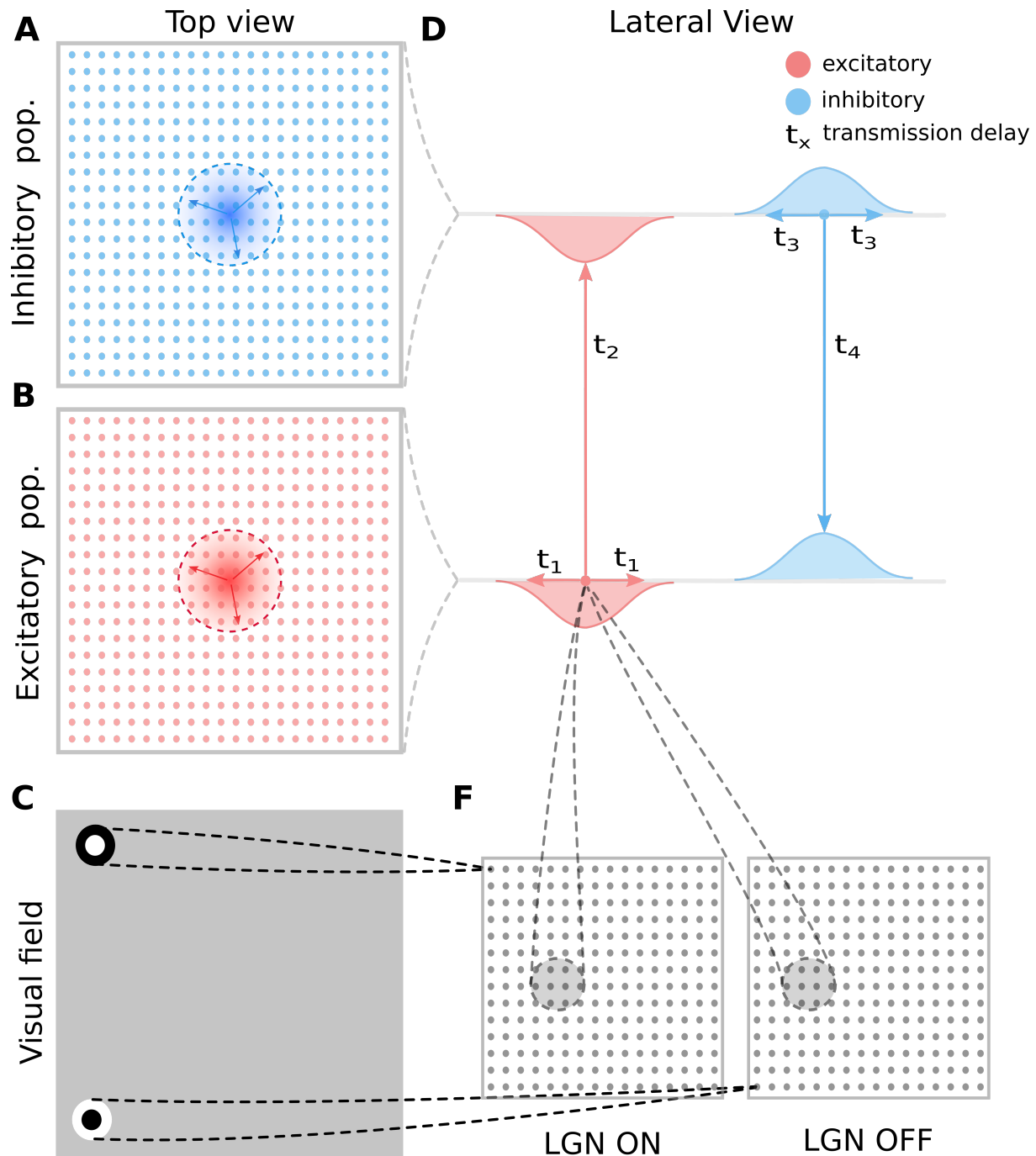


Figure 2. General model architecture. (A) The inhibitory cortical population corresponds to a regular lattice of units in cortical space. (B) As in A but for the excitatory population. (C) Thalamic neurons are modeled as simple difference-of-Gaussian filters followed by a threshold-linear transfer function. (D) The intra-cortical connectivity between the excitatory and inhibitory populations and their transmission delays. The intra-cortical connectivity is the only aspect of the general architecture presented here that changes between the different model variants explored in this study and each variant is detailed in figure 3. (F) The RF centers of the LGN neurons form a regular lattice across the visual space covered by the model. This retinotopic mapping of connection fields between layers of the model is also maintained in the thalamo-cortical projection (lines between D and F). These thalamo-cortical projections are the only connections in the model that undergo Hebbian adaptation during simulated visually driven development.

79 2.1 GCAL model

80 In sections 3.1 through 3.3 (model 1, 2 and 3; see figure 3) we use the GCAL model (Stevens et al.,
 81 2013) which is the most advanced variant of the LISSOM (Laterally Interconnected Synergetically Self-
 82 Organizing Map) algorithm introduced by Miikkulainen *et al.* (Miikkulainen et al., 2005), which itself is
 83 based on earlier Self-Organizing Map models (Kohonen, 1982).

84 For clarity and consistency the following model description closely follows the methodology sections
 85 in our previous work (Stevens et al., 2013; Antolík and Bednar, 2011). The architecture of the 3 GCAL
 86 variants presented in this paper is depicted in figure 2 and figure 3A-C. The models are implemented in the
 87 Topographica simulator, freely available at www.topographica.org. Each of the GCAL models consists of a
 88 set of sheets of model neural units, corresponding to: (1) the photoreceptors, (2) the combined effects of
 89 the retinal ganglion cells (RGC) and ON and OFF LGN cells. Furthermore each model has one V1 sheet
 90 of units with direct excitatory and inhibitory interactions (model 1; see figure 3), or two V1 sheets, one
 91 corresponding to excitatory and one to inhibitory neurons (model 2 and 3; see figure 3). The model sheet
 92 is a 2D array of computational elements (called units or, loosely, neurons), with activation and plasticity
 93 equations as described below and referenced by a coordinate system we will refer to as sheet coordinates,
 94 where the center of the sheet is designated (0.0,0.0). The number of units simulated in each sheet is
 95 determined by the density of units per unit length in both sheet dimensions. All cortical sheets have nominal
 96 dimensions ??×?? in sheet coordinates. The sizes of the RGC/LGN (??×??) and photoreceptor (??×??)
 97 sheets were chosen to ensure that each unit in the receiving sheet has a complete set of connections, thus
 98 minimizing edge effects in the RGC/LGN and V1 sheets. The density of units per 1.0×1.0 area is ??×??
 99 for the photoreceptor and RGC/LGN ON and OFF sheets, and ??×?? for both cortical sheets.

100 2.1.1 Simulation run-time and stimuli

101 As a simplification, GCAL ignores the detailed temporal properties of the sub-cortical neural responses
 102 and of signal propagation along the various types of connections. Instead, the model ON/OFF units have a
 103 constant, sustained output, and all connections have a constant delay, independent of the physical length of
 104 that connection. The simulator operates in discrete time steps. Retinal input changes every ?? time steps
 105 (and during this period is kept constant), and therefore afferent inputs to the V1 sheet(s) are effectively
 106 updated every ?? steps. This process is a discrete simulation of an otherwise continuous series of changes
 107 in membrane potential due to incoming spikes and consequent generation of spikes. One such training
 108 iteration (?? steps) in the model represents one visual fixation i.e., an iteration consists of a constant retinal
 109 activation, followed by processing at the ON/OFF and cortical levels.

110 The activation value ψ_i of unit i in the photoreceptor sheet (P) is given by the gray-scale value in the
 111 chosen image at that point. In this study we use two-dimensional elongated Gaussian patterns, whose
 112 center coordinates and orientation are sampled from a uniform distribution that covers the area of the
 113 photoreceptor sheet and the full range of orientations. Every ?? time steps ?? Gaussian patterns are
 114 superimposed to form the visual input.

115 2.1.2 The LGN/RGC ON and OFF sheets

116 The ON/OFF units are called RGC/LGN units because they represent the entire pathway between the
 117 retinal photoreceptors and V1, including the retinal ganglion cells, LGN cells, and the connection pathways.
 118 The activation level for a unit at position j in an RGC/LGN sheet at time t is defined as:

$$\eta_j(t) = f \left(\frac{A_j(t)}{c + \gamma_L \sum_k A_k(t) l_{kj}} \right) \quad (1)$$

119 where

$$A_j(t) = \gamma_F \sum_{i \in F_j} \Psi_i(t) \omega_{ij} \quad (2)$$

120 The activation function f is a half-wave rectifying function that ensures positive activation values, constant
 121 $\gamma_F = ??$ defines the overall strength of the afferent connections from the retina, constant $\gamma_L = ??$ defines
 122 the strength of the lateral connections within the RGC/LGN sheet, constant $c = ??$ defines the slope of
 123 the gain, Ψ_i is the activation of unit i taken from the set of photoreceptors from which RGC/LGN unit
 124 j receives input (its connection field F_j), ω_{ij} is the connection weight from unit i in the retina to unit j
 125 in the RGC/LGN, and l_{kj} is the lateral connection weight from RGC/LGN unit k to RGC/LGN unit j .
 126 Weights from the photoreceptors to units in the ON and OFF channels are set to fixed strengths with a
 127 difference-of-Gaussians kernel ($\sigma_{center} = ??$, $\sigma_{surround} = ??$, in sheet dimensions), with ON connection
 128 fields having a positive center and a negative surround and vice versa for OFF. The lateral RGC/LGN
 129 weights are 2D Gaussians with kernel size $\sigma = ??$. The center of the afferent and lateral connection field
 130 of each ON/OFF unit is mapped to the location in the photoreceptor and LGN sheet corresponding to the
 131 location of that unit in sheet coordinates, making all these projections retinotopic.

132 2.1.3 Cortical model

133 Units in the cortical sheets each receive three types of projections represented as matrices of weights:
 134 afferent excitatory ($p = A$), lateral excitatory ($p = E$) and lateral inhibitory ($p = I$). The contribution C_{jp}
 135 to the activation of unit j in a cortical sheet from each projection p at time t is given by:

$$C_{jp}(t + \delta t) = \sum_{i \in F_{jp}} \Psi_i(t) \omega_{pij} \quad (3)$$

136 where $\Psi_i(t)$ is the activation of unit i taken from the set of units in the input sheet of projection p from
 137 which unit j receives input (its connection field F_{jp}), and ω_{pij} is the connection weight from unit i in the
 138 input sheet of projection p to unit j in the output sheet of projection p . All connection field weights are
 139 initialized with uniform random noise multiplied by a 2D Gaussian profile, cut off at the distance specified
 140 below. Contributions from each projection are weighted and summed and passed via a non-linearity f to
 141 calculate the activation of a cortical neuron i at time t :

$$\Psi_i(t) = f\left(\sum_p \gamma_p C_{ip}(t)\right) \quad (4)$$

142 where γ_p is a constant determining the sign (negative for inhibitory) and strength of projection p . The
 143 transfer function f is a half-wave rectifying function that ensures positive activation values. It has a variable
 144 threshold point (θ) dependent on the average activity of the unit as described in the next subsection, but
 145 in all cases the gain is fixed at unity. The projection strength scaling factor of the afferent projection γ_A
 146 was set to 1.5 based on Stevens *et al.* (Stevens et al., 2013) while the values of the lateral excitatory and
 147 inhibitory scaling factors, γ_E and γ_I respectively, were varied (see figure 4) to find a balance between
 148 excitation and inhibition, and between afferent and lateral influences, to provide robust formation of activity
 149 bubbles that facilitates the formation of smooth maps.

150 Once all ?? settling steps are complete, the settled cortical activation pattern is deemed to be the response
 151 of cortical sheets to the presented pattern. At this point we use the response of cortical neurons to update
 152 their threshold point (θ) (using the adaptation process described below) and to update the afferent weights

153 via Hebbian learning. Cortical activity is then reset to zero, and a new pattern is presented. Note that both
 154 adaptation and learning could instead be performed at every settling step, but this would greatly decrease
 155 computational efficiency.

156 2.1.4 Homeostatic adaptation

157 The threshold θ of all cortical excitatory units is updated at the end of each settling phase based on the
 158 following equations:

$$\theta_{t+1} = \theta_t + \xi(\tilde{\Psi}(t) - \mu) \quad (5)$$

159 where $\xi = ??$ is the time constant of the threshold adaptation, $\mu = ??$ is a constant defining the target
 160 average activity, and $\tilde{\Psi}$ is the recent average activity of the unit:

$$\tilde{\Psi}(t) = (1 - \chi)\Psi(t) + \chi\tilde{\Psi}(t - 1) \quad (6)$$

161 where $\Psi(t)$ is the output of the unit at time t and $\chi = ??$ is a time constant controlling the decay of the
 162 influence of the past activities. The effect of this scaling mechanism is to bring the average activity of
 163 each cortical unit closer to the specified target. If the activity in a V1 unit moves away from the target
 164 during training, the threshold for activation is thus automatically raised or lowered to bring it closer to the
 165 target. Note that an alternative rule with only a single smoothing parameter (rather than ξ and χ) could be
 166 formulated, but the rule as presented here makes it simple for the modeler to set a desired target activity.

167 2.1.5 Hebbian adaptation

168 The initial connection field weights are isotropic 2D Gaussians for the lateral excitatory projection and
 169 uniformly random within a Gaussian envelope for afferent and lateral inhibitory projections. Specifically, a
 170 neuron located at (i, j) will have the following weights in projection p:

$$\omega_{ijp} = \frac{1}{Z_p} u \exp\left(-\frac{x^2 + y^2}{2\sigma_p^2}\right) \quad (7)$$

171 where (x, y) is the sheet-coordinate location of the presynaptic neuron, $u = 1$ for the lateral excitatory
 172 projection ($p=E$), and u is a scalar value drawn from a uniform random distribution for the afferent and
 173 lateral inhibitory projections ($p=A, I$), σ_p determines the width of the Gaussian in sheet coordinates
 174 ($\sigma_A = 0.27, \sigma_E = 0.035, \sigma_I = 0.035\sqrt{2}$), and Z_p is a constant normalizing term that ensures that the total
 175 of all weights ω_{ijp} to neuron j in projection p is 1.0. Weights for each projection are only defined within a
 176 specific maximum circular radius r_p ($r_A = 0.27, r_E = 0.15, r_I = 0.15\sqrt{2}$).

177 In the model, as images are presented to the photoreceptors, the cortical afferent connection weights $\omega_{i,j,A}$
 178 from the ON/OFF sheets are adjusted once per iteration (after cortical settling is completed) using a simple
 179 Hebbian learning rule. This rule results in connections that reflect correlations between the presynaptic
 180 ON/OFF unit activities and the postsynaptic cortical response. Hebbian connection weight adjustment at
 181 each iteration is dependent on the presynaptic activity, the postsynaptic response, and the Hebbian learning
 182 rate:

$$\omega_{ijA}(t) = \frac{\omega_{ij}(t-1) + \beta_p \Psi_j(t) \Psi_i(t)}{\sum_{p \in \{ON, OFF\}} \sum_k (\omega_{kj,p}(t-1) + \beta_p \Psi_j(t) \Psi_k(t))} \quad (8)$$

183 where β_p is the Hebbian learning rate for the connection fields in the two afferent projections from
 184 RGC/LGN $p \in \{\text{ON}, \text{OFF}\}$. I.e., the afferent weights from RGC/LGN are normalized jointly. Learning
 185 rate parameters are specified as a fixed value $\iota_p = ??$ for each projection, and then the unit-specific values
 186 used in the equation above are calculated as $\beta_p = \frac{\iota_p}{v_p}$, where v_p is the number of connections per connection
 187 field in projection p . The base parameters described here correspond to the first model variant (figure 4).
 188 Any modifications of these base parameters in the other two GCAL model variants 2 and 3 (figure 5,6)
 189 examined in sections 3.2 and 3.3 are then reported in the respective sections.

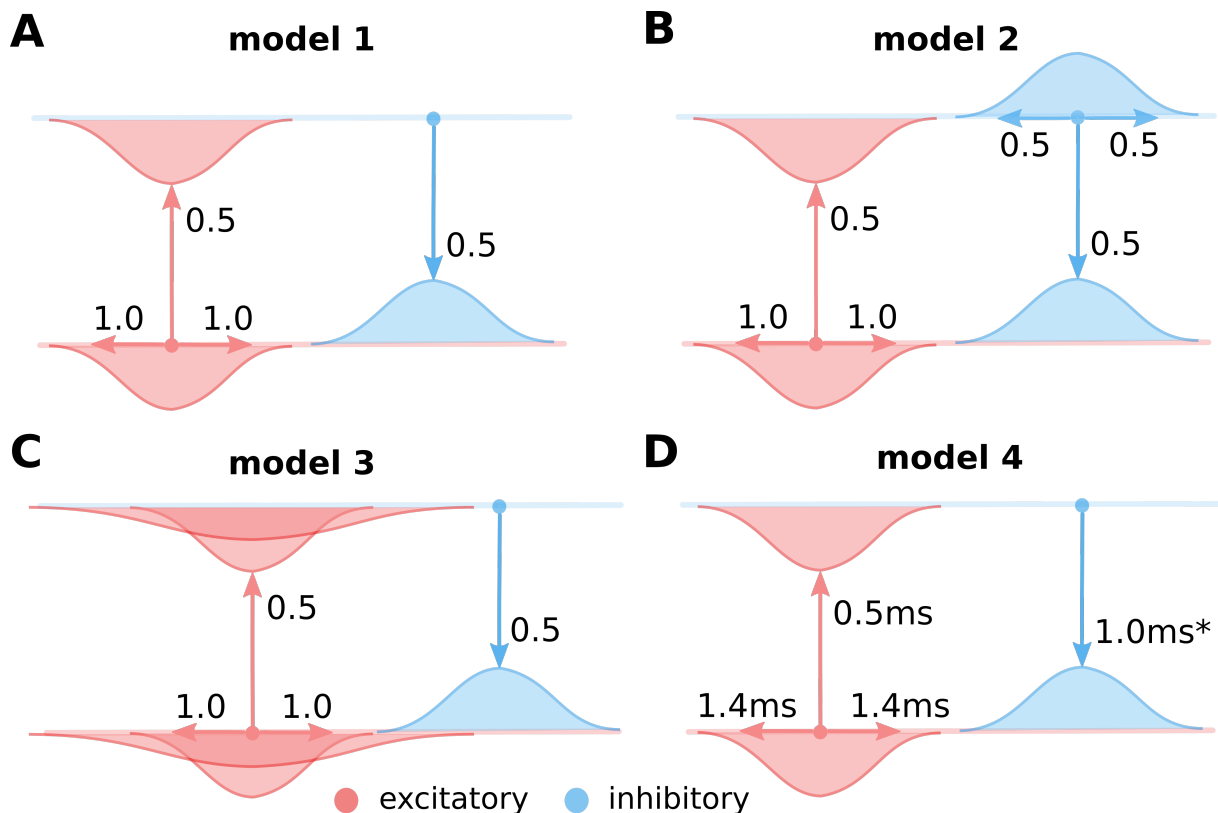


Figure 3. The four considered intra-cortical connectivity variants. As in figure 2, in all panels, the top line represents the excitatory and the bottom line the inhibitory population of neurons. Models (A-C) are using firing rate models of neural units with instantaneous translation of inputs into membrane-potential (see section 2.1). (A) Variant 1, assuming only local equally wide excitatory and inhibitory connectivity, and ignoring direct inhibitory to inhibitory interactions. (B) Variant 2, as in A but with added direct inhibitory to inhibitory connections of equal extent as the other excitatory and inhibitory projections. (C) Variant 3, as in A but with added long-range excitatory connections represented based on Buzás *et al.* (Buzás *et al.*, 2006) as a second wider Gaussian. (D) The same as A but modeled with neural units that take into account membrane time-constant (see section 2.2). The transmission delay of the inhibitory to excitatory projections in model 4 was varied in the experiments presented in section 3.4 (figure 7).

190 2.2 Rate model with membrane time constant

191 The architecture of this model (model variant 4; figure 2 and 3D) is identical to the GCAL models (model
 192 variants 1 through 3; figure 3A-C) with the exception of the equations 3 and 4, which were replaced with
 193 an equation taking into account the membrane time constant:

$$\tau_z \frac{\delta \Psi_i}{\delta t} = -\Psi_i + \sum_p \gamma_p \sum_{j \in F_{ip}} f(\Psi_j(t - \nu_p)) \omega_{pji} \quad (9)$$

194 where τ_z ($z \in \{E, I\}$) is the membrane time constant of excitatory and inhibitory neurons ($\tau_E = ??$ ms,
 195 $\tau_I = ??$ ms), and ν_p is the transmission delay for projection p ($\nu_{EE} = ??$ ms, $\nu_{EI} = ??$ ms, ν_{IE} was varied
 196 (see section 3.4)). As a consequence the evolution of the network dynamics has to be simulated at higher
 197 resolution. We chose the update step to be ??ms, and we let the activity in the model settle for ??ms, thus
 198 resulting in ?? settling steps as opposed to the ?? of the GCAL model. The sub-cortical parametrization
 199 of the model is identical to the model variants 1-3 (figure 3A-C), but because the addition of membrane
 200 time constants substantially changes the cortical dynamics the cortical parameters had to be re-adjusted.
 201 Specifically the strength of the thalamo-cortical connections was set to $\gamma_A = ??$, the strength of the lateral
 202 excitatory-to-excitatory connections was set to $\gamma_{EE} = ??$, the strength of the lateral excitatory-to-inhibitory
 203 connections was set to $\gamma_{EI} = ??$, and the strength of the lateral inhibitory-to-excitatory connections was
 204 set to $\gamma_{IE} = ??$.

205 2.3 Orientation map analysis

206 Model orientation maps are calculated based on the vector average method (Miikkulainen et al., 2005).
 207 We first determine the preferred frequency of neurons across the map. Due to the simplified stereotypical
 208 stimulus used in this study (elongated Gaussian inputs) the spatial frequency preference of all neurons lies
 209 in a very narrow band, and we thus use the mean preferred spatial frequency across all cortical neurons as
 210 the value for the spatial frequency parameter across all subsequent analysis. Next, sinusoidal grating inputs
 211 that cover the full range of remaining parameter values (combinations of all orientations and phases) are
 212 presented, and for each orientation, the peak response of the neuron is recorded. The orientation preference
 213 is calculated by constructing a vector for each orientation θ (between 0 and 180°), with the peak response
 214 as the length and θ as its orientation. These vectors are summed and the preferred orientation is calculated
 215 as half of the orientation of the summed vector. The selectivity is given by the magnitude of the summed
 216 vector.

217 2.4 Orientation map quality measure

218 In order to assess whether the proposed model develops orientation maps that match the structure of those
 219 found in real animals we need to utilize an automatic metric that tells how close the maps are to animal
 220 data. To this end we will utilize a map-quality metric that we have recently developed (Stevens et al., 2013)
 221 based on the empirical observation that pinwheel count in biological orientation maps scales linearly with
 222 hypercolumn size across many different species (Kaschube et al., 2010). Specifically the pinwheel density
 223 per hypercolumn area (Λ^2) converges to π , when averaged across a sufficiently large cortical surface. For a
 224 detailed description of the procedure for calculating this metric we refer the reader to our previous work
 225 (Stevens et al., 2013), but briefly, its calculation involves three steps. First, the locations of the pinwheels
 226 in the orientation map are determined as the intersections of the zero contours of the real and imaginary
 227 components in the polar representation of the maps, thus yielding the total pinwheel count in the map.
 228 Second the hypercolumn size is determined as the peak in the isotropic ring-like Fourier transform of the

229 orientation maps. Third, using these two numbers we can derive the pinwheel density, but to transform
230 it to a useful metric between unity (high-quality map) and zero (low quality map) we pass it through a
231 normalized Gamma distribution. We have shown that this metric reliably distinguishes low and high quality
232 maps (Stevens et al., 2013) and is a valid measure for assessing how well the model orientation maps match
233 animal data.

3 RESULTS

234 In this article we will proceed through multiple gradually more complex models of orientation development,
235 addressing several of the major issues with modeling this phenomenon, eventually demonstrating that the
236 experimentally identified fast inhibitory loop is a satisfactory explanation for how short-range inhibition
237 can support the development of cortical functional organization. We will use two different computational
238 abstractions to explore the questions at hand. In the fist part of the study we will use a computational
239 model that is derived from the LISSOM family of models (Miikkulainen et al., 2005). This choice has three
240 advantages. It allows for a very straightforward explanation of why a fast inhibitory loop enables short-
241 range inhibition to induce competition. It makes our explanation directly comparable to the extensive set of
242 published LISSOM family models, and thus demonstrates that the solution proposed here generalizes to a
243 range of other functional properties. And finally the LISSOM abstraction enables very fast simulations, thus
244 allowing us to perform a parameter search analysis that would otherwise be computationally prohibitive.
245 However, as we will explain further in section 3.4, some simplifications made by the LISSOM abstraction,
246 specifically the instantaneous translation of the neuronal input into its activity, will leave certain questions
247 unanswered. These will be addressed in section 3.4 using more detailed rate model framework.

248 3.1 A fast excitatory to inhibitory to excitatory loop enables competition in networks 249 with short-range inhibitory connections.

250 Ohana *et al.* (Ohana et al., 2012) have shown that transmission delays between different types of cortical
251 neurons are not uniform, specifically they found that on average the transmission delays between excitatory
252 neurons are ~ 1.4 ms, from excitatory to inhibitory neurons are ~ 0.5 ms, and from inhibitory to excitatory
253 neurons are ~ 0.98 ms. The sample size for connections between inhibitory cells in the study was not large
254 enough to be quantitatively reliable. The key observation here is that the combined di-synaptic delay from
255 excitatory to inhibitory and inhibitory to excitatory cells is approximately as long as the mono-synaptic
256 delay of the excitatory to excitatory connections. Drawing from this, the core insight of this study is
257 that under such a pattern of delays the effective inhibitory interactions are well approximated by the
258 convolution of the excitatory and inhibitory connection kernels, as we will show below. This gives the
259 effective inhibition longer range, consequently fulfilling the essential requirement for cortical competition
260 to occur. For didactic purposes, and to simplify analytical treatment, let us first explore one specific set
261 of conditions under which the above statement holds exactly, we will explore the situation when these
262 conditions are relaxed in subsequent sections:

- 263 1. The sum of the excitatory to inhibitory and inhibitory to excitatory delays is exactly the same as the
264 excitatory to excitatory delay
- 265 2. There is no inhibitory to inhibitory interaction
- 266 3. The synaptic inputs into the excitatory and inhibitory neurons are instantaneously translated into their
267 rate response via a positive rectified transfer function.

- 268 4. The connection kernels of all neurons are Gaussian kernels with spatial constant σ_e for excitatory
 269 neurons and σ_i for inhibitory neurons.
 270 5. We will assume only local connectivity (disregarding long-range excitatory connections), and assume
 271 that both excitatory and inhibitory neurons have the same extent, thus $\sigma_e = \sigma_i$

These conditions lead to the following set of equations governing the cortico-cortical interaction.

$$\begin{aligned} R_e(x, t) &= \left[\sum_y N_{\sigma_e}(\|y - x\|) R_e(y, t - \theta_{EE}) - N_{\sigma_i}(\|y - x\|) R_i(y, t - \theta_{IE}) + I_{aff}(x, t) \right]^+ \\ R_i(x, t) &= \left[\sum_y N_{\sigma_e}(\|y - x\|) R_e(y, t - \theta_{EI}) \right]^+ \end{aligned} \quad (10)$$

- 272 where $R_p(x, t)$ is the response of a neuron of type p located at position x at time t , $I_{aff}(x, t)$ is the afferent
 273 input to a neuron at position x at time t , N_σ is a normal distribution of variance σ , corresponding to the
 274 lateral connection kernel, and θ_{ab} is a delay on connections from neural type a to neural type b . When we
 275 expand for R_i we obtain:

$$\begin{aligned} R_e(x, t) &= \left[\sum_y N_{\sigma_e}(\|y - x\|) R_e(y, t - \theta_{EE}) - \sum_y N_{\sigma_i}(\|y - x\|) \left[\sum_z N_{\sigma_e}(\|z - y\|) R_e(z, t - \theta_{EI} - \theta_{IE}) \right] \right. \\ &\quad \left. + I_{aff}(x, t) \right]^+ \end{aligned} \quad (11)$$

- 276 Because $\theta_{EI} + \theta_{IE} = \theta_{EE}$ (assumption 1) and because the inhibitory neurons receive only excitatory
 277 connections (assumption 2) we can further simplify the above as:

$$R_e(x, t) = \left[\sum_y N_{\sigma_e}(\|y - x\|) R_e(y, t - \theta_{EE}) - \sum_z \sum_y N_{\sigma_i}(\|y - x\|) N_{\sigma_e}(\|z - y\|) R_e(z, t - \theta_{EE}) + I_{aff}(x, t) \right]^+ \quad (12)$$

- 278 and thus due to the symmetry of the normal distribution:

$$R_e(x, t) = \left[\sum_y N_{\sigma_e}(\|y - x\|) R_e(y, t - \theta_{EE}) - \sum_z N_{\sigma_i} * N_{\sigma_e}(\|z - x\|) R_e(z, t - \theta_{EE}) + I_{aff}(x, t) \right]^+ \quad (13)$$

- 279 Because convolution of two Normal distributions of variance σ_i and σ_e is a normal distribution with
 280 variance $\sqrt{\sigma_i^2 + \sigma_e^2}$ and because $\sigma_i = \sigma_e$ we can simplify to:

$$R_e(x, t) = \left[\sum_y N_{\sigma_e}(\|y - x\|) R_e(y, t - \theta_{EE}) - \sum_z N_{\sqrt{2}\sigma_e}(\|z - x\|) R_e(z, t - \theta_{EE}) + I_{aff}(x, t) \right]^+ \quad (14)$$

This shows that under these specific assumptions the effective inhibitory interactions between excitatory neurons are $\sqrt{2}$ longer than the excitatory ones and thus follow the Mexican-hat like profile required for the lateral cortical competition underlying functional map development. Even though this essential condition of cortical competition is fulfilled in this model configuration, important constraints on the extent of the effective lateral interactions (relative to lateral excitation) remain. It is thus still unclear whether development of high-quality orientation maps as observed experimentally is supported under these conditions. Conveniently, the lateral interaction in the LISSOM family of models is governed by the same equations as 10. In the following we will use the GCAL model (Stevens et al., 2013), the latest and most robust addition to the LISSOM family of models to demonstrate that the above specific configuration of effective lateral excitation and inhibition permits the development of high-quality orientation maps. GCAL is the only model of stimulus dependent functional development which achieves emergence of biologically realistic orientation maps in terms of pinwheel density, a signature that is a useful objective measure of orientation map quality. We will utilize this map quality measure to reliably detect model configurations which permit the successful emergence of orientation maps. To facilitate a comparison we will use exactly the same model configuration as in Stevens *et al.* (Stevens et al., 2013) (see Materials and Methods), except for three modifications necessitated by the analysis above (see figure 3A):

1. We will change the spread of lateral inhibition to be $\sqrt{2}$ longer than lateral excitatory spread, such that the resulting lateral interactions conform with equation 14.
2. The change in point 1 will result in a change in the balance of overall excitation and inhibition in the model which is critical for successful functional development in the model. We will thus modify the strength of the lateral inhibition to compensate for changes due to modification 1.
3. Analogously to 2, the changes in 1 change the overall balance between feedforward and lateral contributions to model a cortical neuron's activity, which we will compensate by changing the overall strength of the lateral interactions.

In order to find a working combination of parameters in points 2 and 3, and also to show that the model is robust to a certain level of changes in these two parameters, we have performed a parameter search across these two parameters and evaluated the quality of the orientation map (see Materials and Methods) for each parameter combination. As figure 4 shows, under a range of values of both parameters the model develops high-quality orientation maps indistinguishable from their experimental counterparts, thus concluding our first step towards showing that a fast excitatory-to-inhibitory-to-excitatory loop can explain how short-range inhibition can induce cortical competition and consequently the development of topological organization of functional properties.

Furthermore, note that the GCAL model used in figure 4 only explicitly models excitatory neurons and assumes both direct excitatory and inhibitory interactions between them, thus corresponding to equation 14. Even though above we have shown that equation 14 is equivalent to equation 10 to verify the correctness of our analysis we have run a single simulation of the GCAL model corresponding to the parameter combination with the highest map quality found in figure 4, but with an explicitly simulated inhibitory population (figure 4E). In this model we thus do not model direct inhibitory interactions between excitatory neurons, but instead add excitatory to inhibitory and inhibitory to excitatory connections of the same extent as those of the excitatory to excitatory pathway (see the assumption #5). As we have shown above this model should be mathematically equivalent to the simulation shown in figure 4D. Note, however, that the GCAL simulations represent a discrete approximation in both time and space of equations 10,14 and we thus expect small numerical discrepancies. Indeed, orientation maps shown in figure 4E are nearly identical

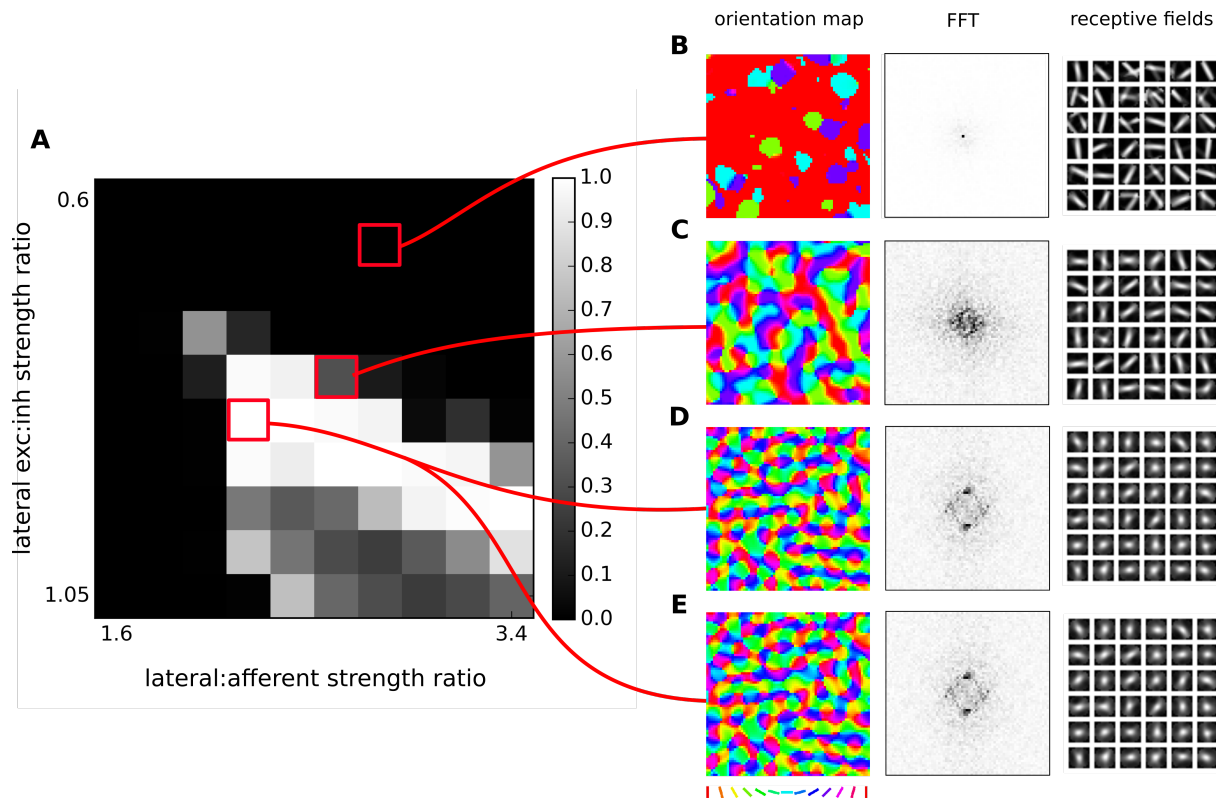


Figure 4. Orientation map development with short range inhibition and a fast excitatory-to-inhibitory-to-excitatory loop. (A) Map quality (see Materials and Methods) at a range of lateral excitatory vs inhibitory projection strength ratios and afferent vs lateral projection strength ratios. (B-D) Functional organization in 3 example parameter configurations indicated by the red marks. From left to right, the orientation map, fast-Fourier transform of the orientation map and afferent connection fields from the ON LGN model sheet for 25 example model V1 neurons. (B-C) Two examples of sub-optimal orientation maps. (D) Model configuration with the highest quality map found in this parameter search. (E) The same model configuration but in this case it was run with explicit simulation of inhibitory neurons and corresponding connections. E and D are nearly identical confirming the correctness of our analysis.

324 to those in the figure 4D, with only barely perceptible numerical differences, confirming the validity of our
325 approach.

326 **3.2 Inhibitory to inhibitory connections are consistent with development of functional
327 organization**

328 In the previous section we have shown that under a set of specific assumptions that facilitate analytical
329 treatment, short-range inhibition can induce effective Mexican-hat like interaction and thus support the
330 development of orientation maps. However, not all assumptions we made were in line with experimental
331 evidence. In this section we will show, now only numerically, that one of these assumptions is not
332 necessary, specifically that the addition of inhibitory to inhibitory connections does not prevent emergence
333 of orientation maps.

334 To this end, we will use the exact GCAL model configuration that we have found in the previous section
335 to possess the highest quality orientation map (see figure 4). We will use the GCAL configuration in which
336 we will explicitly model the inhibitory neurons (see figure 3B, and equation 10) and consequently also
337 explicitly the excitatory to inhibitory and inhibitory to excitatory connections. Furthermore, we will add

338 inhibitory to inhibitory connections to the model with the same extent as that of inhibitory to excitatory
 339 connections ($\sigma_i = \sigma_e$ in eq 10).

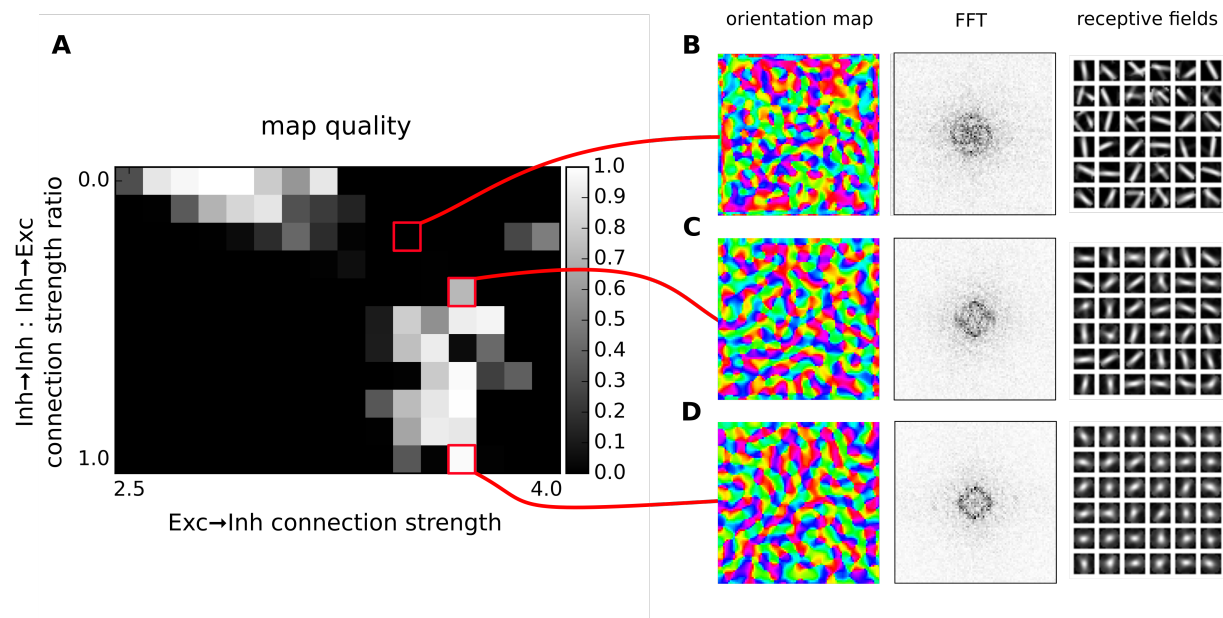


Figure 5. Orientation map development with short range inhibition, a fast excitatory-to-inhibitory-to-excitatory loop and inhibitory to inhibitory connections. (A) Map quality (see Materials and Methods) at a range of inhibitory to inhibitory vs inhibitory to excitatory projection strength ratios and excitatory to inhibitory connection strengths. (B-D) Functional organization in 3 example parameter configurations indicated by the red marks. From left to right, the orientation map, fast-Fourier transform of the orientation map and afferent connection fields from the ON LGN model sheet for 25 example model V1 neurons.

340 By explicitly modeling the inhibitory neurons in this model we have replaced a single parameter governing
 341 the strength of inhibitory lateral interactions in the model from the previous section with three new
 342 parameters that set: (1) the strength of excitatory to inhibitory, (2) inhibitory to excitatory and (3) inhibitory
 343 to inhibitory connections (all other parameters remained the same as the in the best parameterization found
 344 in the previous section). Note that in principle, there is redundancy in these parameters as the overall
 345 strength of the projections from inhibitory neurons onto both excitatory and inhibitory populations is scaled
 346 by the excitatory to inhibitory projection strength. Therefore in figure 5 we have systematically varied the
 347 strength of the added inhibitory to inhibitory projection expressed relatively to the strength of the inhibitory
 348 to inhibitory connections (which was set to 1), while also varying the strength of the excitatory to inhibitory
 349 projection. We have investigated the quality of the orientation maps that developed under these different
 350 levels of inhibitory to inhibitory interactions. As can be seen, high quality maps can develop under the full
 351 range of the inhibitory to inhibitory interaction strengths, depending on the overall excitatory to inhibitory
 352 drive. This shows that inclusion of direct inhibitory to inhibitory interactions does not invalidate the results
 353 of section 3.1 (figure 4).

354 3.3 Long-range excitation

355 In model variants 1 and 2 (figure 4 and 5) we have only assumed local connectivity by setting both
 356 excitatory and inhibitory interactions to have the same spatial extent. However experimental evidence shows
 357 that excitatory cells send longer connections compared to inhibitory cells (Buzás et al., 2006; Budd and
 358 Kisvárdy, 2001). In this section we will explore what happens if we add long-range excitatory connectivity

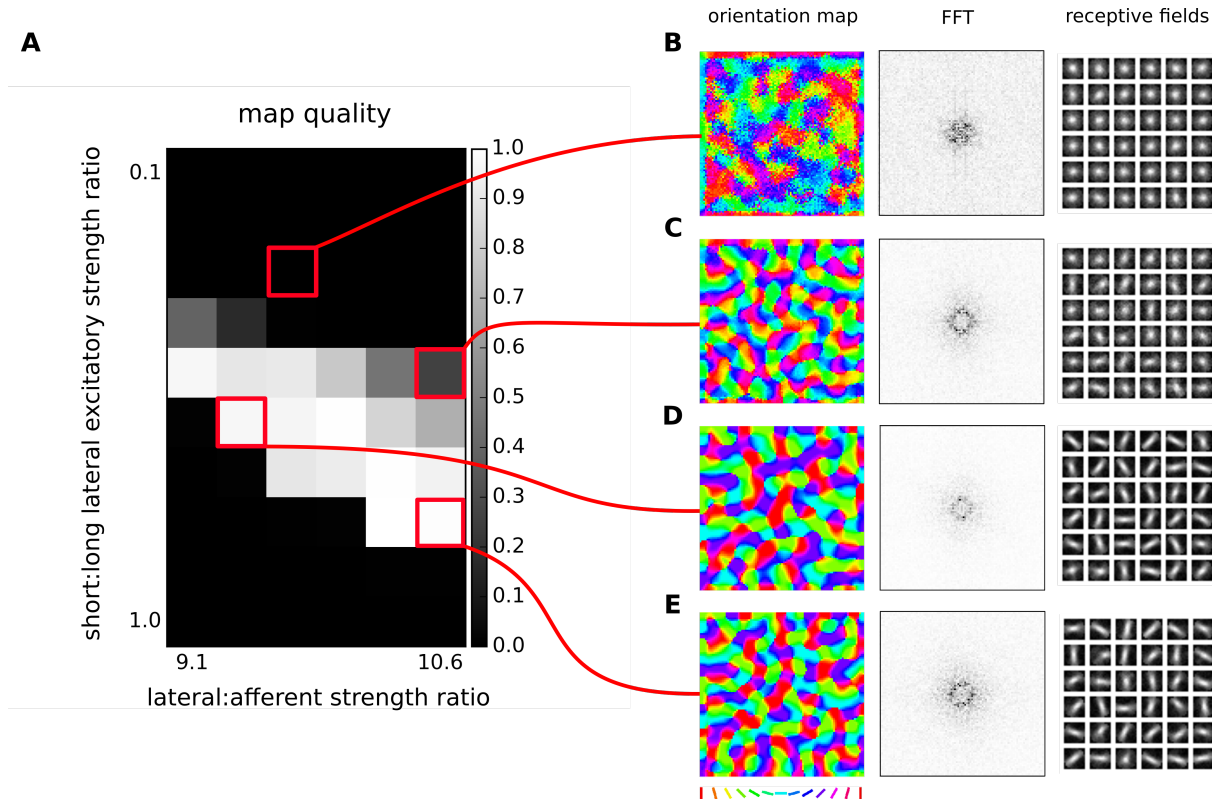


Figure 6. Orientation map development with short range inhibition, a fast excitatory-to-inhibitory-to-excitatory loop and long-range excitation. (A) Map quality (see Materials and Methods) at a range of short vs. long range excitatory connection strength ratios (y-axis) and a range of afferent vs. lateral connection strength ratios (x-axis). (B-E) Functional organization in 4 example parameter configurations indicated by the red marks. From left to right, the orientation map, fast-Fourier transform of the orientation map and afferent connection fields from the ON LGN model sheet for 25 example model V1 neurons.

359 into model variant 1. Buzás *et al.* (Buzás et al., 2006) have shown that the lateral connectivity in layer 2/3
 360 can be best described as superimposition of two gabor connectivity likelihoods, one short-range but not
 361 orientation specific and one long-range and orientation specific. Here we will assume such dual structure,
 362 leading us to add a second excitatory to excitatory and excitatory to inhibitory projection into model variant
 363 1, but with a space constant that is 3 times larger (see figure 3C), in line with Buzás *et al.* (Buzás et al.,
 364 2006) quantitative findings.

365 In figure 6 we will examine what strength of the long-range excitatory connections, relative to the
 366 short-range excitatory ones (y axis in figure 6A), leads to development of a high-quality orientation map.
 367 Adding the long-range excitation changes the spatial configurations over which excitatory interactions win
 368 over inhibitory ones, as well as the overall magnitude of the resulting net local excitation. Consequently,
 369 the proportion between the magnitude of the net local excitation due to the lateral interactions and the
 370 excitation due to afferent inputs is changed, which is a crucial parameter for map development. To
 371 compensate for these changes, we also systematically explore the ratio of the overall magnitudes of
 372 the lateral and afferent interactions (x axis of figure 6). To make the parameter search computationally
 373 feasible, we perform the parameter search only in the region of parameters that allow for sufficiently strong
 374 long-range excitatory projections. As can be seen in figure 6D and E, under appropriately strong lateral
 375 interactions, substantial long-range excitatory connections still permit the development of high quality

376 orientation maps, demonstrating that the proposed model is consistent with the experimentally identified
377 long-range excitatory connectivity.

378 **3.4 Non-equal effective excitatory and inhibitory delays**

379 In all model variants examined so far we have made the key assumption that the delay on the excitatory
380 to excitatory connections is exactly equal to the sum of excitatory to inhibitory and inhibitory to excitatory
381 delays. This assumption is approximately supported by the experimental evidence (Ohana et al., 2012), but
382 we cannot assume it holds exactly in a real biological substrate. However, we hypothesize, that the small
383 discrepancies between the delay of the mono-synaptic excitatory connections and the cumulative delay of
384 the bi-synaptic inhibitory interactions can be absorbed into the membrane time-constant of the neurons.
385 In this section we will verify this hypothesis by extending the modeling framework used thus far with a
386 finite membrane time-constant (see Materials and Methods) and proceed to determine the magnitude of the
387 discrepancy in the delays between the excitatory and inhibitory interactions that can be managed by the
388 model without impairing the resulting orientation map quality.

389 We use a model parameterization similar to those determined for model variant 1 (section 3.1; figure 3A).
390 For simplicity and computational efficiency we omit the inhibitory to inhibitory and long-range excitatory
391 connections that have already been investigated with model variants 2 and 3. The membrane time-constant
392 of excitatory neurons was set to ??ms while those of inhibitory neurons to ??ms. These faster inhibitory
393 dynamics are necessary to prevent oscillations in the system (Kang et al., 2003). We set the excitatory to
394 excitatory delay to 1.4 ms and excitatory to inhibitory delay to 0.5 ms based on Ohana *et al.* (Ohana et al.,
395 2012). In order to understand how closely the cumulative bi-synaptic inhibition delay has to match that of
396 the direct excitatory to excitatory delay, we will vary the delay on the inhibitory to excitatory projection
397 (note that we could achieve the same by varying the excitatory to inhibitory delays, and this choice was
398 arbitrary).

399 Figure 7 shows the resulting orientation maps and associated map quality measures of models with a
400 range of differences between the delays of monosynaptic excitatory and bi-synaptic inhibitory interactions,
401 that are in the figure expressed as the sum of the excitatory to inhibitory and inhibitory to excitatory
402 delays minus the excitatory to excitatory delay (i.e. the figure shows how much slower the inhibitory
403 disynaptic interactions were in comparison with the monosynaptic excitatory ones). As can be seen when
404 the differences between the excitatory delay (1.4ms) and cumulative inhibitory delay is small (<0.8 ms)
405 high quality orientation maps develop in the model, confirming that sufficiently large discrepancy between
406 the direct excitatory and bi-synaptic inhibitory delays can be accommodated in the model. However, as
407 expected, as the difference between the delays increases the ability of the model to learn a topologically
408 organized representation of orientation preference diminishes. Crucially, if the delays across all the
409 projections were equal (figure 7), as is typically assumed, the model fails to develop orientation maps
410 in line with the analysis by Muir *et al.* (Muir and Cook, 2014), thus confirming that the specific delay
411 pattern between neural types identified by Ohana *et al.* (Ohana et al., 2012) is key to achieving competitive
412 dynamics in topologically organized neural models.

4 DISCUSSION

413 In this study we have shown how recent findings on dependence of neural transmission delays on the type
414 of pre- and post-synaptic neurons (Ohana et al., 2012) can resolve a long-standing question on how short-
415 range inhibition can support cortical competition and consequently the development of functional cortical
416 topological organization. Under simplifying assumptions, we have analytically shown how disynaptic

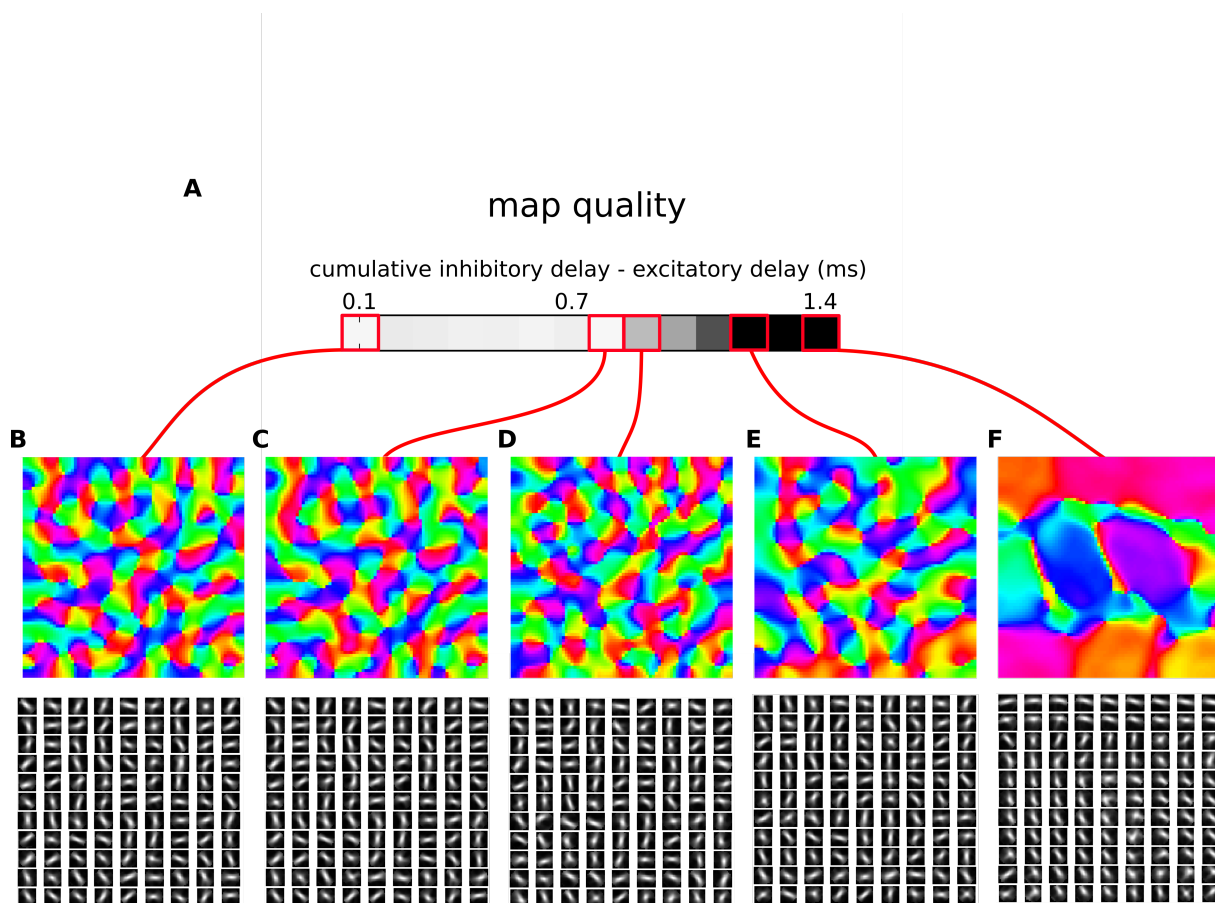


Figure 7. Orientation map development in a rate model with a synaptic time constant. (A) Map quality (see Materials and Methods) at a range of cumulative inhibitory delays expressed as the difference from the direct excitatory to excitatory delays. (B-F) Functional organization in 5 parameter configurations indicated by the red marks. The orientation map (top), and afferent connection fields from the ON LGN model sheet for 81 example model V1 neurons (bottom). (B-D) Three examples of configurations where good quality orientation maps develop. (E) If the cumulative inhibitory delay is longer by more than approximately 0.8ms in comparison to the direct excitatory delay the map quality starts to drop. (F) In the configuration corresponding to the case where delays on all connections are equal (i.e. the cumulative delays of the inhibitory interactions is twice as long as on the direct excitatory ones) orientation maps fail to develop.

417 inhibition that is as fast as mono-synaptic excitation can extend the effective range of inhibitory interactions,
 418 in contrast to the recent analytical results showing that in the case of equal synaptic delays on all connections
 419 the disynaptic inhibition has negligible effects (Muir and Cook, 2014). We have also shown that these
 420 findings are applicable to the problem of functional development in primary visual cortex. We have then
 421 proceeded to show using computational methods that the proposed models are robust to the addition
 422 of other well established features of cortical anatomy, commonly ignored by similar studies, including
 423 the long-range excitatory connections and mutual inhibition among inhibitory neurons. Finally, we have
 424 shown that the proposed mechanisms are robust to the variations of the exact delay ratio between the
 425 mono-synaptic excitation and di-synaptic inhibition. Overall, this study represents an important advance in
 426 our understanding of how orientation map development can be supported by the cortical neural substrate.
 427 These results generalize to the development of other functional features in the cortex and other cortical
 428 competition based mechanisms in general.

429 The most related past explanation of how cortical competition can arise under short range inhibition is
430 that of Kang *et al.* (Kang et al., 2003), who have shown that under the assumption of a faster inhibitory
431 time constant (as opposed to excitatory), the effective excitatory and inhibitory interactions will follow
432 the Mexican hat profile and thus support competition along the cortical surface. Indeed, in our final
433 model variant 4 that explicitly considers membrane time-constant presented in section 3.4, we assume that
434 inhibitory neurons have faster membrane time constants than excitatory ones, as otherwise we observe
435 oscillatory behavior in line with the analytical findings of Kang *et al.* (Kang et al., 2003). Crucially, Kang *et*
436 *al.* (Kang et al., 2003) assumed instantaneous neural transmission, and when this biologically implausible
437 assumption is rectified by addition of transmission delays that are uniform across the connections between
438 the different pre- and post-synaptic neural types, we find that the competitive dynamics in the neural
439 model break (figure 7F) in line with the analytical and computational results of Muir *et al.* (Muir and Cook,
440 2014). However, when we replace the transmission delays with the neural-type specific pattern uncovered
441 by Ohana *et al.* (Ohana et al., 2012) the competitive dynamics in the model are rescued and we observe
442 development of high quality orientation maps (section 3.4AB), in line with the analytical results under
443 simplified conditions (section 3.1).

444 The analytical results in this study were obtained only under simplifying assumptions, specifically
445 instantaneous translation of inputs to membrane potential, equal extent of excitatory and inhibitory
446 connections and a lack of inhibitory-to-inhibitory interactions. Even though we have shown computationally
447 that these assumptions are not necessary for achieving the cortical competition and the consequential
448 orientation map development sought in this study, further analytical work then can circumvent these
449 simplifications and would undoubtedly provide deeper understanding of the dynamics of the studied neural
450 system and its dependence on the various parameters. This sentiment underlies the parameter explorations
451 presented here, which show that even though the model is robust to changes in the considered parameters,
452 the existence or not of dynamics supporting development of orientation maps forms a complex pattern
453 within the explored parameter spaces. Furthermore, the relative computational complexity of the studied
454 models and the extensive set of parameters involved preclude systematic search across the full parameter
455 space, and we have only explored parameters that we empirically found to have the biggest impact. Finally,
456 one simplifying assumption that we have not treated in this study is the lack of direct thalamic input onto
457 inhibitory cells. Since inhibitory cells in cortical layer 4 do receive thalamic input (Binzegger et al., 2004)
458 the inclusion of external input in the inhibitory population needs to be considered in the future.

459 In this paper we have decided to investigate cortical competitive mechanisms through the prism of
460 orientation map development. The advantage of this approach is that it allows us not only to show that
461 some form of competition is possible, but also that it is of the form that actually supports implementation
462 of specific cortical computations. Given that we show that our model implements effective Mexican hat
463 lateral interactions (section 3.1) and these have in the past been shown to be sufficient to explain cortical
464 organization of other functional features (i.e. retinotopy, ocular dominance, spatial frequency and color) it
465 is very likely that our results will generalize to these other dimensions of sensory input as well. Cortical
466 competition of other forms has been proposed to underly a broad variety of other cortical operations,
467 including associative memory, noise suppression, decision making, saliency detection and other forms of
468 attentional computations. Even though additional work will be required to determine if the mechanisms
469 proposed here can generalize to these other neural computations, this study offers a promising framework
470 for anatomically plausible mechanistic explanations of these important aspects of brain function.

CONFLICT OF INTEREST STATEMENT

471 The authors declare that the research was conducted in the absence of any commercial or financial
472 relationships that could be construed as a potential conflict of interest.

AUTHOR CONTRIBUTIONS

473 JA performed the calculus, simulations and wrote the manuscript.

FUNDING

474 The research leading to these results has received funding from the European Union Seventh Framework
475 Programme (FP7/2007-2013) under grant agreement no. 604102 (Human Brain Project).

ACKNOWLEDGMENTS

476 I would like to thank James A. Bednar and Andrew Davison for reviewing the original draft and providing
477 valuable comments on the presented research.

REFERENCES

- 478 Amit, D. J. and Brunel, N. (1995). Learning internal representations in an attractor neural network with
479 analogue neurons. *Network: Computation in Neural Systems* 6, 359–388. doi:10.1088/0954-898X/6/3/
480 004
- 481 Antolík, J. and Bednar, J. A. (2011). Development of maps of simple and complex cells in the primary
482 visual cortex. *Frontiers in Computational Neuroscience* 5, 1–19. doi:10.3389/fncom.2011.00017
- 483 Ben-Yishai, R., Bar-Or, R. L., and Sompolinsky, H. (1995). Theory of orientation tuning in visual cortex.
484 *Proceedings of the National Academy of Sciences of the United States of America* 92, 3844–3848.
485 doi:10.1073/pnas.92.9.3844
- 486 Binzegger, T., Douglas, R. J., and Martin, K. a. C. (2004). A quantitative map of the circuit of cat primary
487 visual cortex. *The Journal of neuroscience : the official journal of the Society for Neuroscience* 24,
488 8441–53. doi:10.1523/JNEUROSCI.1400-04.2004
- 489 Budd, J. M. and Kisvárday, Z. F. (2001). Local lateral connectivity of inhibitory clutch cells in layer 4 of
490 cat visual cortex (area 17). *Experimental Brain Research* 140, 245–250. doi:10.1007/s002210100817
- 491 Buzás, P., Kovács, K., Ferecskó, A. S., Budd, J. M. L., Eysel, U. T., and Kisvárday, Z. F. (2006).
492 Model-based analysis of excitatory lateral connections in the visual cortex. *The Journal of comparative
493 neurology* 499, 861–81. doi:10.1002/cne.21134
- 494 Durstewitz, D., Seamans, J. K., and Sejnowski, T. J. (2000). Neurocomputational models of working
495 memory. *Nature neuroscience* 3, 1184–1191. doi:10.1038/81460
- 496 Grabska-Barwinska, A. and von der Malsburg, C. (2008). Establishment of a scaffold for orientation maps
497 in primary visual cortex of higher mammals. *The Journal of neuroscience : the official journal of the
498 Society for Neuroscience* 28, 249–57. doi:10.1523/JNEUROSCI.5514-06.2008
- 499 Kang, K., Shelley, M., and Sompolinsky, H. (2003). Mexican hats and pinwheels in visual cortex.
500 *Proceedings of the National Academy of Sciences of the United States of America* 100, 2848–53.
501 doi:10.1073/pnas.0138051100

- 502 Kaschube, M., Schnabel, M., Löwel, S., Coppola, D. M., White, L. E., and Wolf, F. (2010). Universality
503 in the Evolution of Orientatino Columns in the Visual Cortex. *Science* 330, 1113–1116. doi:10.1126/
504 science.1194869.Universality
- 505 Kohonen, T. (1982). Self-organized formation of topologically correct feature maps. *Biological Cybernetics*
506 43, 59–69. doi:10.1007/BF00337288
- 507 Law, J. S. (2009). *Modeling the Development of Organization for Orientation Preference in Primary Visual*
508 *Cortex*. Ph.D. thesis, School of Informatics, The University of Edinburgh, Edinburgh, UK
- 509 Levy, R. B. and Reyes, A. D. (2011). Coexistence of lateral and Co-Tuned inhibitory configurations in
510 cortical networks. *PLoS Computational Biology* 7. doi:10.1371/journal.pcbi.1002161
- 511 Miikkulainen, R., Bednar, J. A., Choe, Y., and Sirosh, J. (2005). *Computational Maps in the Visual Cortex*.
512 (Springer)
- 513 Muir, D. R. and Cook, M. (2014). Anatomical Constraints on Lateral Competition in Columnar Cortical
514 Architectures. *Neural computation* 1872, 1840–1872. doi:10.1162/NECO
- 515 Ohana, O., Portner, H., and Martin, K. a. C. (2012). Fast recruitment of recurrent inhibition in the cat
516 visual cortex. *PLoS ONE* 7. doi:10.1371/journal.pone.0040601
- 517 Rutishauser, U., Slotine, J.-J., and Douglas, R. J. (2012). Competition through selective inhibitory
518 synchrony. *Neural computation* 24, 2033–52. doi:10.1162/NECO__a__00304
- 519 Somers, D. C., Nelson, S. B., and Sur, M. (1995). An emergent model of orientation selectivity in cat visual
520 cortical simple cells. *The Journal of neuroscience : the official journal of the Society for Neuroscience*
521 15, 5448–5465
- 522 Stevens, J.-L. R., Law, J. S., Antolík, J., and Bednar, J. A. (2013). Mechanisms for stable, robust, and
523 adaptive development of orientation maps in the primary visual cortex. *The Journal of neuroscience : the*
524 *official journal of the Society for Neuroscience* 33, 15747–66. doi:10.1523/JNEUROSCI.1037-13.2013
- 525 von der Malsburg, C. (1973). Self-organization of orientation sensitive cells in the striate cortex. *Kybernetik*
526 14, 85–100